Feature Article:
DOI. No. 10.1109/MAES.2017.180054

LTE CommSense for Object Detection in Indoor Environments

***Santu Sardar*, ANURAG, Defence Research & Development Organization, Hyderabad, India**
***Amit K. Mishra*, University of Cape Town, Cape Town, South Africa**
***Mohammed Zafar Ali Khan*, IIT Hyderabad, Hyderabad, India**

INTRODUCTION

In this work, we describe a new method of using long-term evolution (LTE) telecommunication infrastructure to sense environmental changes. We call it LTE communication-based sensing (CommSense). It can be used in various environment-sensing tasks, e.g., sea level monitoring, security of large unmanned landscapes, snow avalanche monitoring, and activity detection inside forests. The main concept of this technology is to focus on the known signal embedded in the data frames. It compares the received signal with the expected reference signal to estimate the change in the environment. LTE telecommunication infrastructure is used for this environment-sensing task because of its wide coverage. In addition, LTE uses a two-dimensional (2D) frame structure of orthogonal frequency division multiplexing (OFDM) and multiple input and multiple output (MIMO), which may yield better performance compared to previous communication standards. This procedure of extracting channel characteristics using commensal radar principles does not affect the existing telecommunication system, because it is a receive-only system. After the channel characteristics are estimated, they can be used to obtain phenomenological knowledge of the environment using an application-specific instrumentation (ASIN) framework. The capability analysis of this scheme is presented in this article, first in simulation and then using field-collected data captured with the help of a software-defined radio (SDR) platform.

The first known work in the open literature using radar for data communication is the U.S. patent by Rittenbach published in 1969 [1]. The field of coexisting telecommunication and radar systems to detect and track targets has been gaining importance. In general, the telecommunication and radar systems share benefits without a detrimental effect between them. This field is commonly known as passive radar or commensal radar [2]–[5].[1] These efforts of coexistence continue for various applications [5], [6].

One interesting way of exploiting the existing telecommunication system is to gather information from the channel estimation blocks in the system. Channel estimation is performed to estimate the effect of a dynamic channel on the unknown data pattern by observing its effect on a known data pattern (reference symbols or pilots). That means the output of a channel estimation block contains channel information. Collectively, the channel properties (scattering, fading, and power decay with distance) of the communication link are known as channel state information (CSI). This CSI is exploited by our proposed CommSense scheme [7], [8]. In the last 2 years, a large amount of work has been done regarding the feasibility of a global system for mobile communications (GSM)-based CommSense system [4].

Our work on developing an LTE-based CommSense system is presented in this article. It has a different set of challenges, possibilities, and applicabilities compared to the corresponding GSM-based system. In this article, we present initial results and analysis of simulation data, as well as practical data captured using an SDR-based LTE CommSense system. Application of the LTE communication standard for communication-based environment sensing is a novel idea. In LTE, the receiver user equipment (UE) is significantly different from GSM-based UE. The motivations for using LTE for CommSense are as follows:

- The existing LTE network is widespread and will grow wider in the near future.
- Because OFDM is basically wideband in nature, it is considered a waveform with low interception probability.
- The wideband nature of OFDM has the ability to overcome fading and multipath problems [9].
- Using the property of frequency diversity, LTE CommSense may provide more information about the scene of interest.

Authors' current addresses: S. Sardar, ANURAG, DRDO, PO Kanchanbagh, Hyderabad, PIN-500058, Telangana, India, E-mail: (sardar.santu@gmail.com). A. K. Mishra, Department of Electrical Engineering, Room 7.07, 7th Floor, Menzies Building, Library Road, Upper Campus, University of Cape Town, Cape Town, South Africa. M. Z. A. Khan, Department of Electrical Engineering, IIT Hyderabad, Sangareddy, Kandi, PIN-502285, Telangana, India.
Manuscript received February 15, 2017, revised May 8, 2017, and ready for publication July 12, 2017.
Refereeing of this contribution was handled by D. O'Hagan.
0885/8985/18/$26.00 © 2018 IEEE

[1] The word commensal is borrowed from ecology.

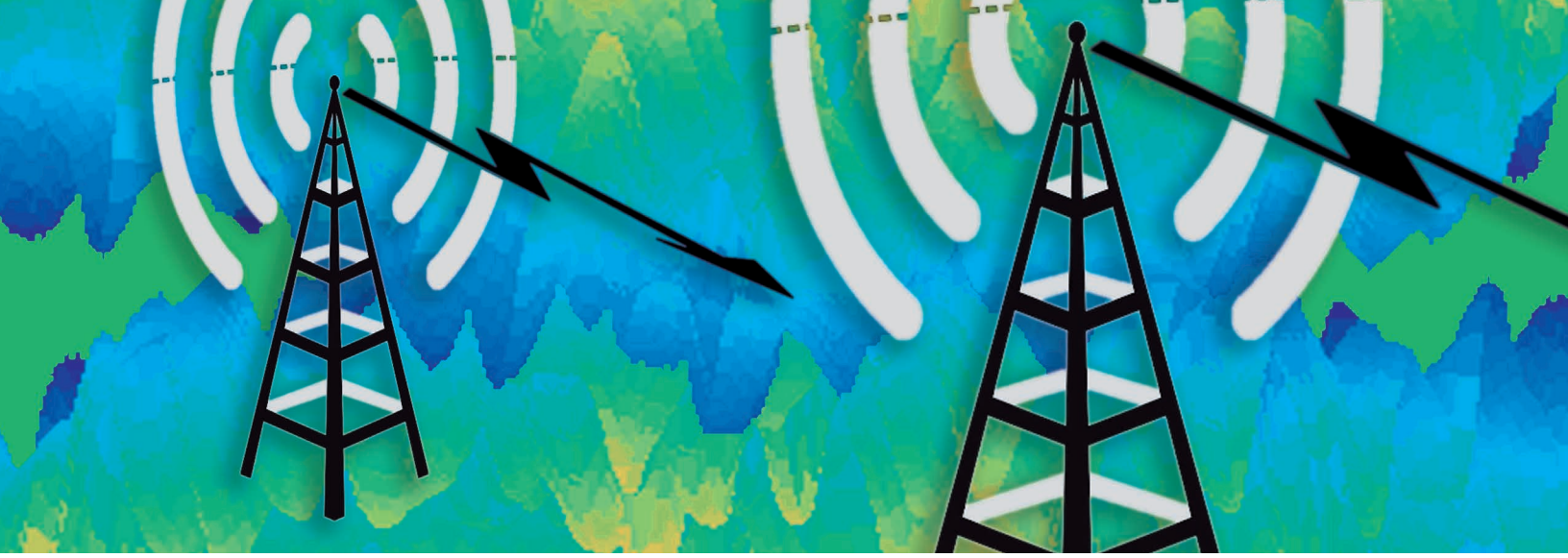

Therefore, LTE is more suitable than any other communication platform for CommSense.

The following results are shown in this article:

- The feasibility of the LTE CommSense instrument is shown using simulation. It is shown that within the limitations of simulation, we can recognize different kinds of International Telecommunication Union (ITU)-specified LTE channels.
- A practical LTE downlink (DL) signal is captured using a CommSense system implemented using an SDR platform and analyzed for intraclass similarity and interclass dissimilarity for different environments. Two types of analyses are performed. After evaluating the channel estimates, the dimension is reduced using principal component analysis (PCA) and plotted for cluster visualization. Then, fractional Fourier transform (FrFT) is performed to analyze their time–frequency representations (TFRs) to investigate whether the user can directly distinguish different scenarios by observing plots of FrFT-processed outputs.
- We show the effect of varying the distance of the target object from the sensing system, i.e., how the sensing performance changes with the distance of the object from the system.

LTE COMMSENSE FORMULATION, SYSTEM DESIGN, AND IMPLEMENTATION

In a telecommunication receiver system, the objective is to estimate the received signal assuming a known channel model. This channel is estimated using a channel estimation block, and the effect of channel irregularity is minimized using the channel equalization block. Channel estimation and equalization blocks of telecommunication systems use various processes, algorithms, and techniques to estimate dynamic, nonergodic, and fading channels in real time and try to nullify the channel effects on the transmitted data. However, in a radar system, the transmitted data are known a priori and the goal is to estimate the channel [8].

CommSense aims to work as a commensal radar and uses telecommunication radiation to estimate the channel information from the channel estimation block. To do this, CommSense taps into the dynamic channel estimation block of a telecommunication system. Telecommunication transmitters transmit reference pilot symbols at regular intervals. The channel-distorted version of the reference symbols received at the receiver provides information about the channel conditions. Based on the preceding observations, we have proposed that the CommSense system [7], [8] will successfully do the following:

- Estimate the channel characteristics from the received telecommunication signal.
- Predict the change in the environment based on the change in the channel characteristics.

For successful operation of CommSense, i.e., to perform the preceding tasks, mapping of information from the channel estimation measurements to environment events or conditions is crucial. This may be thought of as a phenomenological effort, which is a major challenge in conventional radar systems [10]. Therefore, this is a major concern in our proposed LTE CommSense system as well.

LTE COMMSENSE SYSTEM

CommSense can be implemented with the help of any telecommunication system that sends pilot signals for channel estimation and equalization. Work on GSM-based CommSense systems [4], [5] show promising results. The current work focuses on implementing CommSense using LTE technology, which is a new standard of choice for cellular telecommunication. The main motivations for using LTE for CommSense were listed in the introduction.

Figure 1 shows the complete processing chain of the proposed LTE CommSense system. Because two sets of inputs are required, there are two separate processing chains. The first one is during operational mode, when real-time data are input from UE deployed in the environment. UE is an LTE receiver. It captures the DL signal from an LTE base station and initiates the receiver processing chain. The second chain is required during the control mode. In

this mode, the control center sets the information and processing depending on the purpose of the LTE CommSense.

The process blocks (PBs) in the processing chains are as follows:

1. Process-block-1 (PB-1): Channel information is extracted from channel estimation and/or equalization blocks. Multiple UEs may be used to increase area coverage in the future. If multiple UEs are used, the channel estimates of every individual UE will be passed to PB-2.
2. Process-block-2 (PB-2): All information from individual UEs of PB-1 are fused to pass on to PB-3. In this article, a single piece of UE is used. Therefore, PB-2 is bypassed.
3. Process-block-3 (PB-3): Information is gathered regarding the event that has to be detected. This is passed to the ASIN block in PB-4 to train the ASIN framework.
4. Process-block-4 (PB-4): The ASIN classifier is trained with the information from PB-3. After that, it detects events using information from PB-1 and PB-2.
5. Process-block-5 (PB-5): The user is informed about the decision of the ASIN block. Information will mainly comprise confirmation of event occurrence and/or event details (in case the event occurrence likelihood is estimated to be high by ASIN).

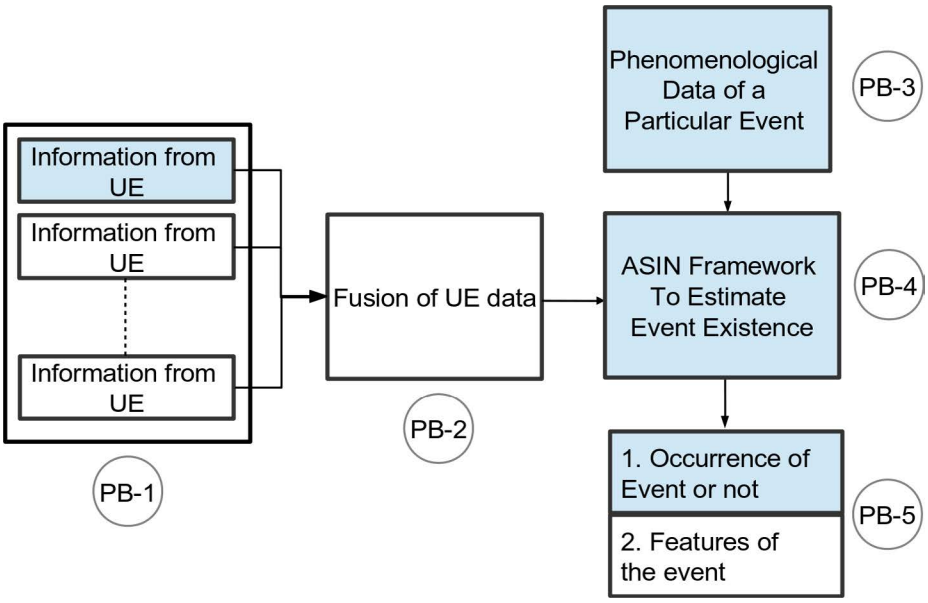

Figure 1.
Different stages in the processing chain of an LTE CommSense system.

The ASIN framework [11] is used to obtain phenomenological knowledge about the environment. ASIN is a bioinspired instrumentation scheme that aims to estimate one or a few changes only, instead of trying to estimate everything in the scene.

First, we prove the hypothesis in simulation, and then we prove it using practical data. To capture practical data, i.e., live LTE DL signals from LTE base stations, the LTE receiver is implemented in the Universal Software Radio Peripheral (USRP) N200 SDR platform. The simulation and experiment details, data-capturing methods, processing, and analysis are explained next.

EXPERIMENTS AND ANALYSIS

VERIFICATION IN THE SIMULATION ENVIRONMENT

To validate our hypothesis using simulation, we considered additive white Gaussian noise (AWGN) added to different ITU-specified LTE channel models [12]. Then, the corresponding CSI was evaluated and passed to a pattern classifier to verify the feasibility of whether the same models can be used to distinguish the channels.

We first modeled the LTE resource grid and then modeled different ITU-specified channel models for LTE and applied them, along with AWGN, to the transmitted signal. The LTE resource grid is a multicarrier OFDM signal arranged in the form of frames. A resource element (RE) is an element of the time–frequency grid. It is a single modulation symbol for a single subcarrier. Combined together, REs form resource blocks (RBs). A single RB contains 12 subcarriers. For each subcarrier, 6 or 7 OFDM symbols are included. The number of OFDM symbols depends on the cyclic prefix (CP) mode (normal or extended). The system bandwidth in the frequency domain is an integer multiple of RBs.

Four ITU-specified channel models were considered here: ITU extended pedestrian A (EPA), ITU extended vehicular A (EVA), ITU extended typical urban (ETU), and no multipath fading condition. The multipath profile of EPA, EVA, and ETU channel models [12] are shown in Table 1. These are the types of channel conditions typically encountered for LTE telecommunication. Using the LTE CommSense model, we tried to distinguish these types of channel conditions. To perform this, first we determined the CSI from the LTE receiver for different LTE channel models and fed it to a simple nearest-neighbor (NN) classifier. Corresponding confusion matrices are also recorded.

Furthermore, we analyzed the effect of signal-to-noise ratio (SNR) on the classification performance by observing the corresponding root mean square error vector magnitude (RMS EVM) at different SNR values. The classification performance was observed at low SNR values ranging from −7 to 0 dB.

Simulation Setup

The highlighted blocks in Figure 1 are implemented in this analysis. A single UE is considered. Therefore, fusion of data in PB-2 is not considered here.

Table 1.

ITU-Specified Channel Models Compatible with LTE Telecommunication Used for Verification of LTE CommSense in Simulation Environment

Tap No.	EPA		EVA		ETU	
	Relative Delay (ns)	Relative Mean Power (dB)	Relative Delay (ns)	Relative Mean Power (dB)	Relative Delay (ns)	Relative Mean Power (dB)
1	0	0.0	0	0.0	0	–1.0
2	30	–1	30	–1.5	50	–1.0
3	70	–2	150	–1.4	120	–1.0
4	80	–3	310	–3.6	200	0.0
5	110	–8	370	–0.6	230	0.0
6	190	–17.2	710	–9.1	500	0.0
7	410	–20.8	1,090	–7	1,600	–3.0
8	—	—	1,730	–12	2,300	–5.0
9	—	—	2,510	–16.9	5,000	–7.0

The stagewise processing block diagram describing the extraction procedure of LTE CSI is shown in Figure 2. The channel estimation algorithm functions are described in the following steps:

1. Extract the reference signals, or pilot symbols, for a transmit–receive antenna pair from the received grid. Use the reference signals to calculate the least-squares estimates of the channel response at the pilot symbol positions within a received grid.
2. To minimize the effects of noise on the pilot symbol estimates, average the estimates using an averaging window. This simple method produces a substantial reduction in the level of noise found on the pilot symbols.
3. Using the cleaned pilot symbol estimates, generate virtual pilots to facilitate interpolation at the boundaries of the LTE resource grid.
4. Interpolate to obtain an estimate of the channel for the entire number of subframes passed into the function.

The received resource grid is compared between the transmitted and equalized grids and the transmitted and received grids . The errors between the transmitted and the equalized grids and the transmitted and the received grids are calculated in terms of RMS EVM. The CSI is extracted and recorded.

Results and Analysis

The extracted CSIs for all four models used for analysis are plotted in Figure 3. The x-axis gives the subcarrier numbers, the y-axis

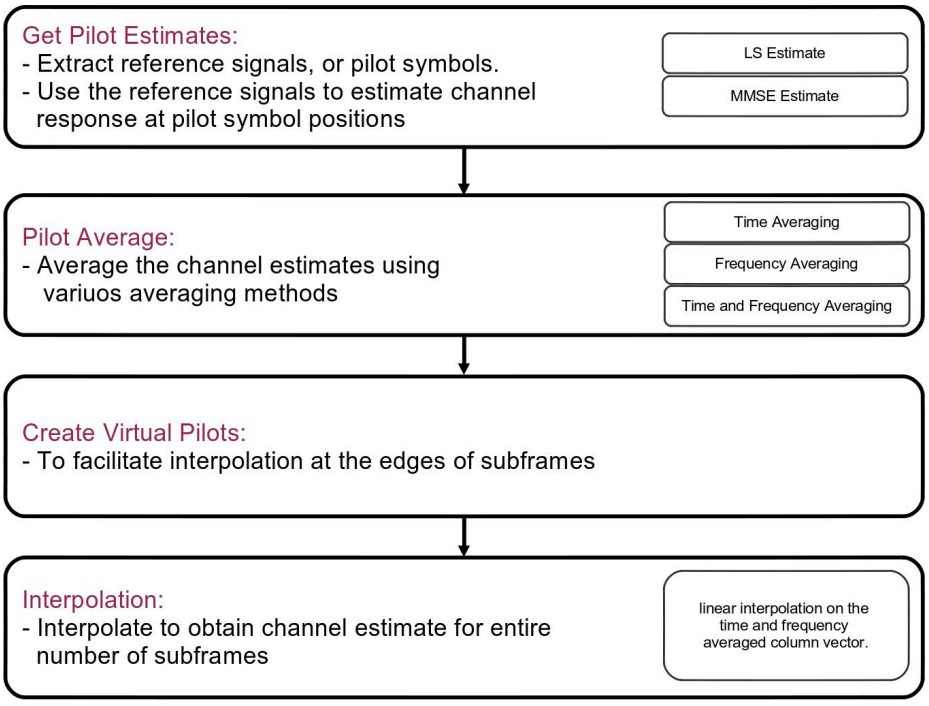

Figure 2.
LTE channel estimation and CSI extraction block diagram.

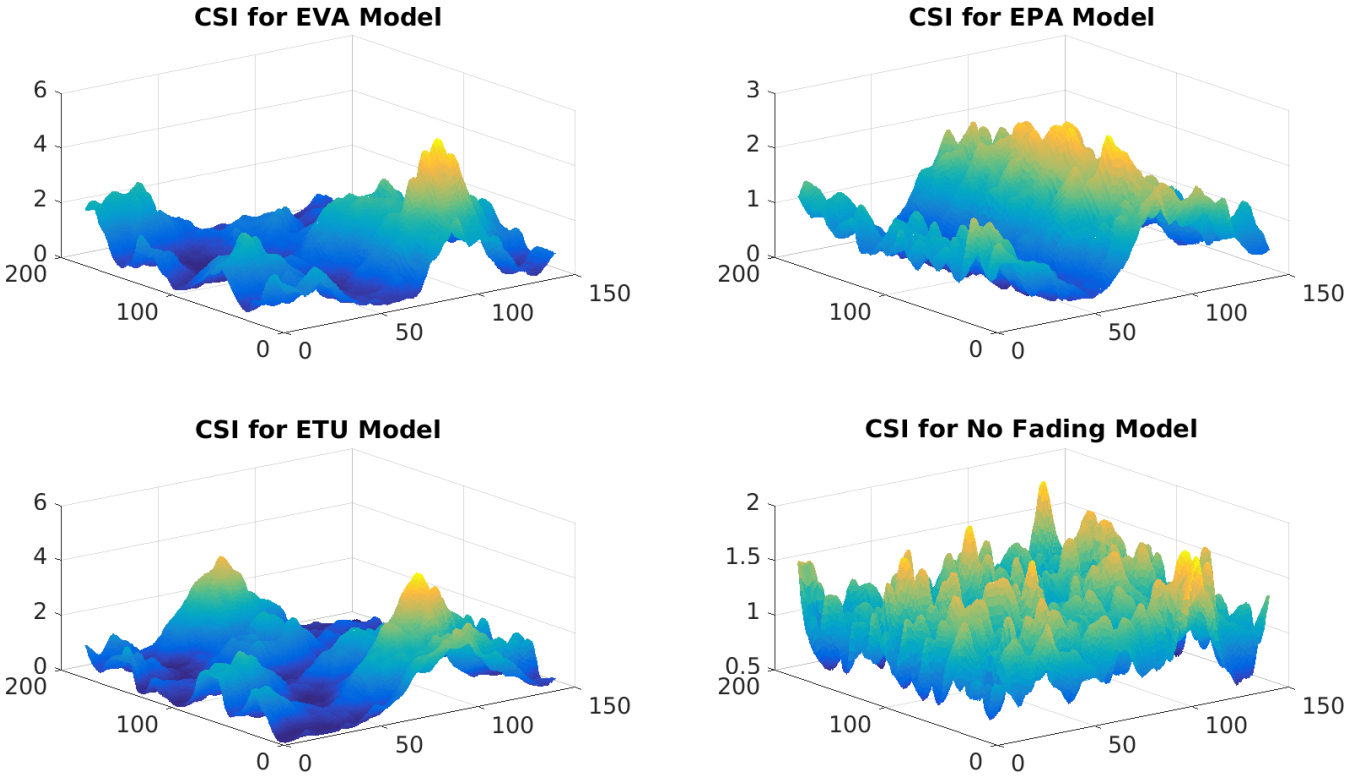

Figure 3.
CSI extracted from the LTE channel estimator block for four fading channel models.

Table 2.

LTE CommSense Performance Accuracy and Corresponding Confusion Matrix for Different SNR Values

SNR (dB)	Accuracy (%)	Confusion Matrix				SNR (dB)	Accuracy (%)	Confusion Matrix			
–7	73	35	5	10	0	–3	98.5	50	0	0	0
		0	43	7	0			0	50	0	0
		0	0	50	0			0	0	50	0
		1	20	11	18			0	2	1	47
–6	84	47	1	2	0	–2	100	50	0	0	0
		0	47	3	0			0	50	0	0
		0	0	50	0			0	0	50	0
		0	18	8	24			0	0	0	50
–5	88.5	49	0	1	0	–1	100	50	0	0	0
		0	47	3	0			0	50	0	0
		0	0	50	0			0	0	50	0
		0	13	6	31			0	0	0	50
–4	94	49	0	1	0	0	100	50	0	0	0
		0	49	1	0			0	50	0	0
		0	0	50	0			0	0	50	0
		0	7	3	40			0	0	0	50

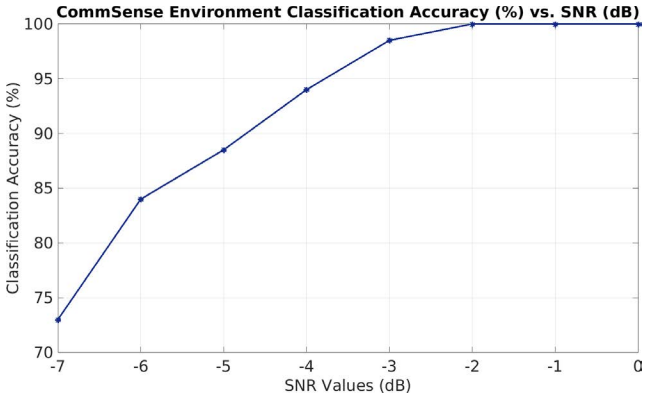

Figure 4.
LTE CommSense performance accuracy to distinguish ITU-specified channel models at different SNR values in the simulation environment.

represents the OFDM symbol, and the z-axis is the corresponding value of the CSI in this time–frequency grid. It can be observed that the CSIs for different channel models are different.

In the next stage, the feasibility of using these CSIs to obtain knowledge about the environment is investigated using an NN classifier. Later, this simple classifier may be replaced with better classifiers to further increase the performance. Euclidean distance is considered as the distance measure in the classifier. For a single SNR value, 50 readings were recorded for each of the channel models to generate the training dataset. The test dataset was created accordingly. Similarly training and testing data were generated for other SNR values as well. Given the CSI, the classifier determines to which channel model in the training dataset it best corresponds. Multiple SNR values were considered to evaluate the CommSense performance at different SNR levels, as shown in Table 2.

The accuracy vs. SNR plot for this CommSense analysis is shown in Figure 4. It can be observed that even at negative SNR values, we get more that 80% classification accuracy.

It can be concluded that different channel models corresponding to different types of fading channels, as specified by ITU for LTE, are recognizable using the CSI obtained at the receiver. This proves the claim that CommSense is feasible using LTE infrastructure. The performance is observed and found to be satisfactory at low SNR conditions even using the NN pattern classifier. The classification performance may improve further using a better classifier.

EXPERIMENTAL SETUP

In the next stage, we used practical data for the analysis. To capture a real-time LTE DL signal, OpenLTE, an open-source, GNU Radio-based implementation of the 3rd Generation Partnership Project (3GPP) LTE specifications, was used on the USRP N200 platform [13]. We used OpenLTE version 00-19-00 [14]. We modeled the LTE receiver on the USRP N200 platform using OpenLTE, which complies with the LTE specifications. A photo of the data-capturing device N200 in action is shown in Figure 5a, and its block diagram is shown in Figure 5b. Along with the N200 platform, the RFX2400

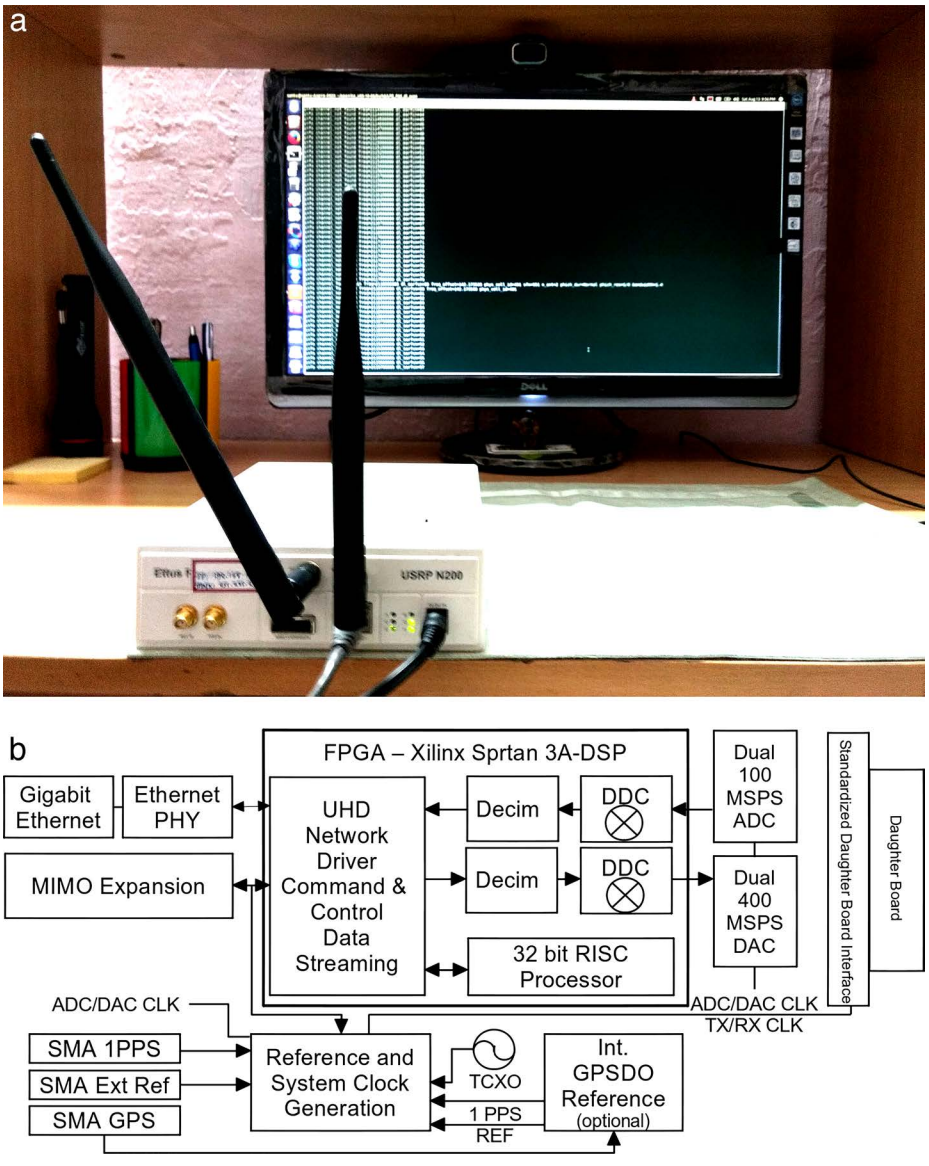

Figure 5.
(a) USRP N200 data-capturing device (front) and host PC screen showing the detected LTE channel by use of OpenLTE. (b) USRP N200 internal block diagram.

RF daughter card [15] is used, which operates in the range of 2.3–2.9 GHz. The VERT2450 antenna [16], which operates in the LTE passband frequency range, is used with the daughter card.

The received signal is compared to the expected signal to estimate the change in the environment.

Description of Captured Data

According to the LTE frame structure, one frame has a 10-ms duration and consists of 10 individual subframes, each with a duration of 1 ms. These data will be in complex (in-phase and quadrature [I-Q]) format. Each subframe is mapped with a cell-specific reference signal and primary and secondary synchronization signals. Therefore, after evaluating channel estimates from an LTE frame, we can shift by one frame to get a new set of readings from the real-time LTE DL recording and evaluate another channel estimate. Because one recording of LTE DL data is captured for 15 s, we can evaluate up to 1,500 channel estimates from 1,500 readings from a single recording using the preceding procedure. If LTE DL data are captured for more than 15 s, a higher number of channel estimates can be computed accordingly.

ANALYSIS OF CAPTURED DATA

After the LTE DL data are captured using the modeled LTE receiver in the USRP SDR platform [13] and channel estimates are evaluated for specific experimental scenarios, they are processed to visualize and distinguish the differences and infer environment changes because of possible target presence or absence. Two types of analysis were performed, viz. PCA [17] for dimensionality reduction followed by cluster analysis and FrFT to analyze TFRs of the channel estimates.

To perform cluster analysis, the higher-dimension data were first reduced to the lower two or three dimensions and plotted in scatterplot. PCA was used to perform dimensionality reduction. The superiority of PCA for many uses is established in [17]. PCA involves a procedure that transforms a number of (possibly) correlated variables into a (smaller) number of uncorrelated variables called principal components.

To perform PCA, first the covariance matrix of the dataset was calculated as follows:

$$F = \left(\frac{1}{N}\right) * \left(x_k - v\right)\left(x_k - v\right)^T, \tag{1}$$

where $v = \overline{x_k}$ is the mean of the data and N is equal to the number of elements in the dataset. PCA is based on the projection of correlated high-dimensional data onto a hyperplane. This mapping uses only the first few q nonzero eigenvalues and the corresponding eigenvectors of the covariance matrix $F_i = U_i \Lambda_i U_i^T$, where Λ_i is a diagonal matrix whose entries are the eigenvalues $\lambda_{i,j}$ of F_i in decreasing order and the matrix U_i includes the eigenvectors corresponding to the eigenvalues in its columns. The vector $y_{i,k} = W^{-1}\left(x_k\right) = W^T\left(x_k\right)$ is a q-dimensional reduced representation of the observed vector x_k, where the W_i weight matrix contains the q principal orthonormal axes in its column $W_i = U_{i,q}\Lambda_i^{\left(\frac{1}{2}\right)}$.

As an alternative data visualization method to readily detect environment changes from their processed plots, FrFT processing was also explored. Information about this topic can be found in [18]. FrFT (also called rotational Fourier transform or angular Fourier transform) can be considered a rotation by angle α (not a multiple of $\pi/2$) in the time–frequency plane or a decomposition of the signal in terms of chirps. The FrFT was computed using the angle of rotation in the time–frequency plane as the fractional power of the ordinary Fourier transform. Letting $x(u)$ be an arbitrary signal, its ath-order FrFT is defined as [18]

$$X_a\left(u\right) = \int k_a\left(u,u'\right)x\left(u'\right)du', \tag{2}$$

where a is the fractional transformation order (corresponding to a rotation angle $\alpha = a\pi/2$, with $a \in \Re$). a is a unitless scalar quantity; its value ranges from 0 to 4, so the value of α can range from 0 to 2 * π radian. $k_a(u,u')$ is the FrFT kernel and is defined as

$$k_a\left(u,u'\right) = \begin{cases} A_0 * \exp\left[j\pi\left(\left(u^2 + u'^2\right) * \cot\left(\alpha\right) - 2uu' * \csc\left(\alpha\right)\right)\right] \\ \alpha \neq n * \pi, n \in I \\ \delta\left(u - u'\right); \alpha = n * 2 * \pi, n \in I \\ \delta\left(u + u'\right); \alpha + \pi = n * 2 * \pi, n \in I \end{cases};$$

where $A_0 = \dfrac{e^{\frac{\alpha}{2}}}{\sqrt{j * \sin\left(\alpha\right)}}$.

The applicability of FrFT for visual feature extraction using TFRs is established in [19] in the case of synthetic aperture radar (SAR) automatic target recognition (ATR). For LTE CommSense, the channel estimates are obtained in the time–frequency grid. These channel estimates were analyzed using their corresponding TFRs to find consistent visual differences for data visualization and inference.

Lastly, we show the performance change of CommSense with respect to distance of the object from the CommSense system.

Cluster Analysis

The objective of this phase was to establish the feasibility of detecting human targets in an indoor environment using cluster analysis. Though the scope of this work is to detect a human target in an indoor environment, the capability of detecting other objects can be explored. The dimensions of the captured channel estimates were reduced using PCA and plotted in two and three dimensions for visual analysis. We investigated whether we can differentiate

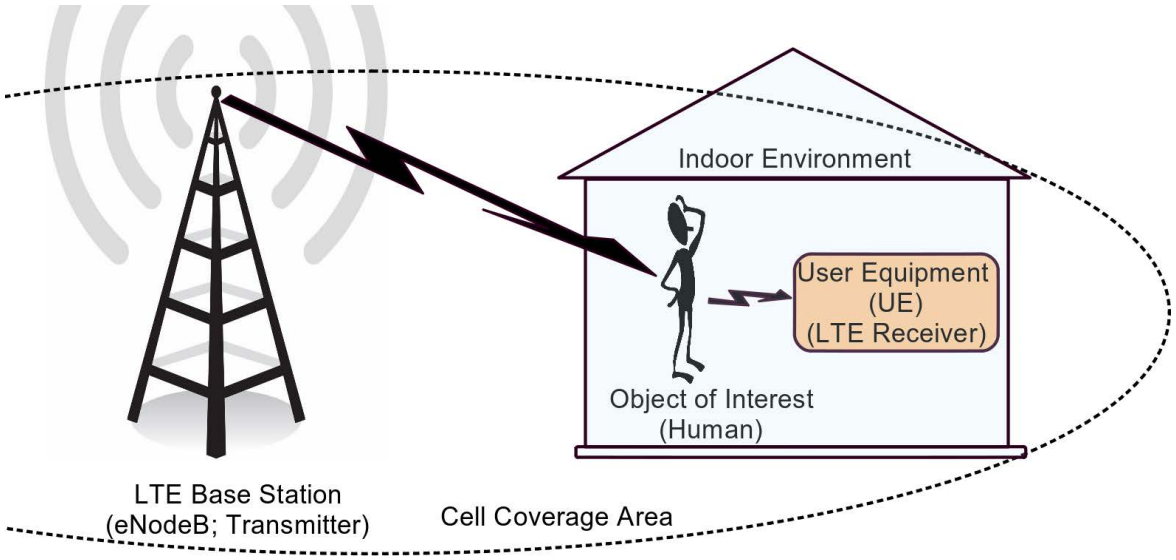

Figure 6.
Floorplan representing the position of the receiver, person, and transmitter for indoor human-target detection using the CommSense experiment.

clusters with and without a human in an indoor environment from the scatter plots. The following experimental procedure was adopted for this purpose:

1. Six indoor environments were chosen.
2. LTE DL signals were captured with and without the human target for the six backgrounds. A floorplan depicting the position of the receiver, person, and transmitter is shown in Figure 6.
3. The distance of the human target from the USRP device was kept constant. The human target was placed 2.5 m from the SDR platform, which is working as an LTE receiver. Figure 7 shows the different indoor environments with the target object.
4. For all preceding cases, data were divided into two categories: with and without target.
5. The channel estimate for all cases were evaluated.
6. PCA was performed on the channel estimates to reduce its dimension.
7. Support vector machine (SVM)-based classification of the reduced dataset was performed.

Figure 8 shows the PCA results of the received data captured using USRP N200 working as an LTE receiver. The dimension of the data was reduced using PCA. To select how many prin-

Figure 7.
Different indoor environments used for the invariant human-target detection experiment. LTE DL data recordings are performed in these five backgrounds with and without the human target.

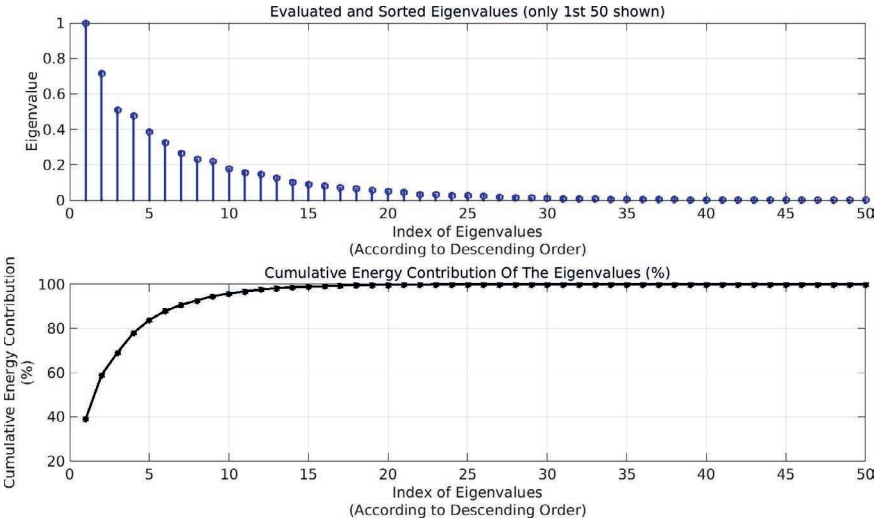

Figure 8.
Sorted eigenvalues and their cumulative energy contribution for indoor human-target detection.

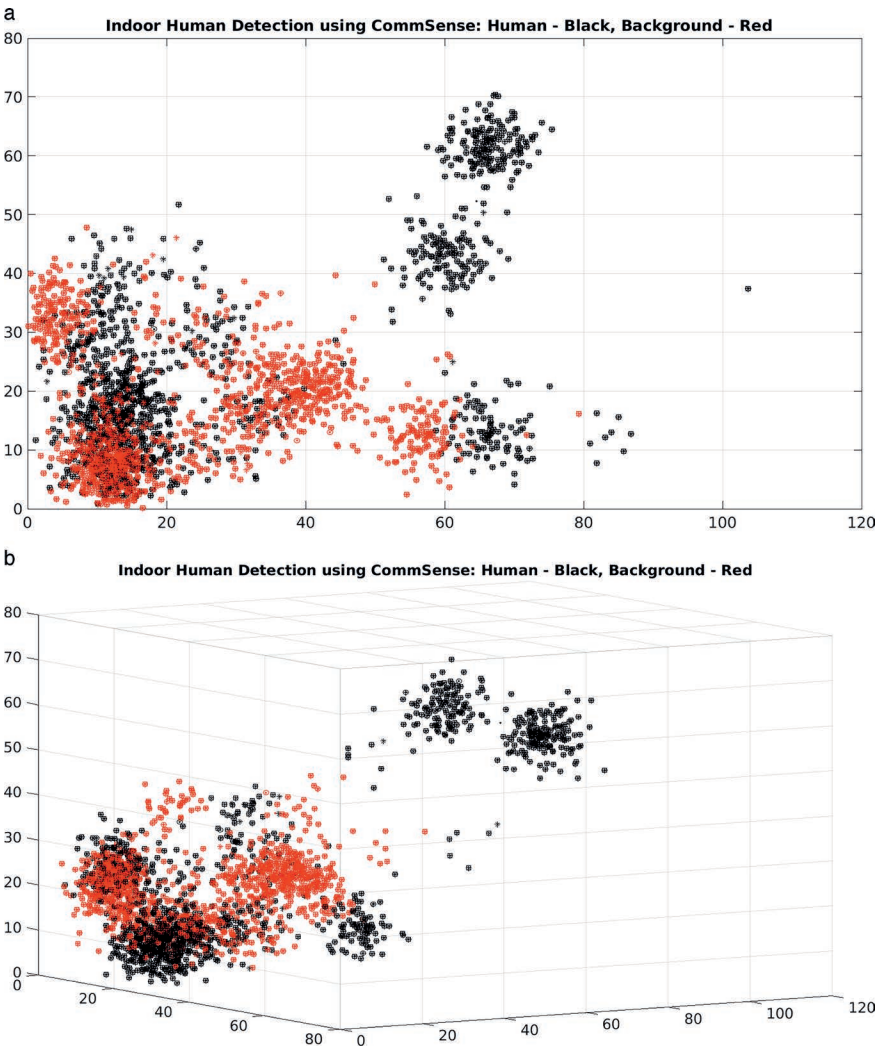

Figure 9.
Indoor human-target detection using cluster analysis: (a) 2D scatterplot of the largest two principal components, (b) 3D scatterplot of the largest three principal components.

cipal components are sufficient for this case to faithfully represent the variability of the input data, the sorted eigenvalues and their cumulative energy contribution are plotted in Figure 8. It can be observed that the values of the eigenvalues gradually decrease and that after the 35th eigenvalue, the magnitudes of other eigenvalues are negligible. Consequently, the cumulative energy contribution of the eigenvalues saturates after the 35th eigenvalue. This information is required to reduce the dimension of the data while preserving the variability. Before passing the data to the pattern classifier, dimension reduction following the preceding procedure may be performed for efficient computation. The largest two principal components are plotted in a 2D scatterplot and shown in Figure 9a. The three-dimensional (3D) scatterplot of the largest three principal components is shown in Figure 9b. In the scatterplots in Figure 9, the red cluster points correspond to indoor backgrounds and black cluster points represents indoor backgrounds with the human target present.

It can be observed that clusters with and without a human target are distinct. Hence, it can be concluded that the human target can be detected in indoor environments using the CommSense system.

Visualization and Inference

FrFT was performed on the channel estimates to investigate whether distinguishing features can be observed directly from the plots of the processed estimates. The channel estimates with and without a human target in an indoor environment in the FrFT domain are shown in Figure 10. The top row of the figure shows multiple channel estimates for the with-human case, and the bottom row shows channel estimates for the without-human case.

We observed the individual TFRs and selected the corresponding TFR, which shows the most consistent distinctive features. Figure 11 shows the TFRs for different rotation angles for both the cases, i.e., with and without human. Although in all images, the difference between the first- and the second-row images for a particular angle is visible, it is prominent

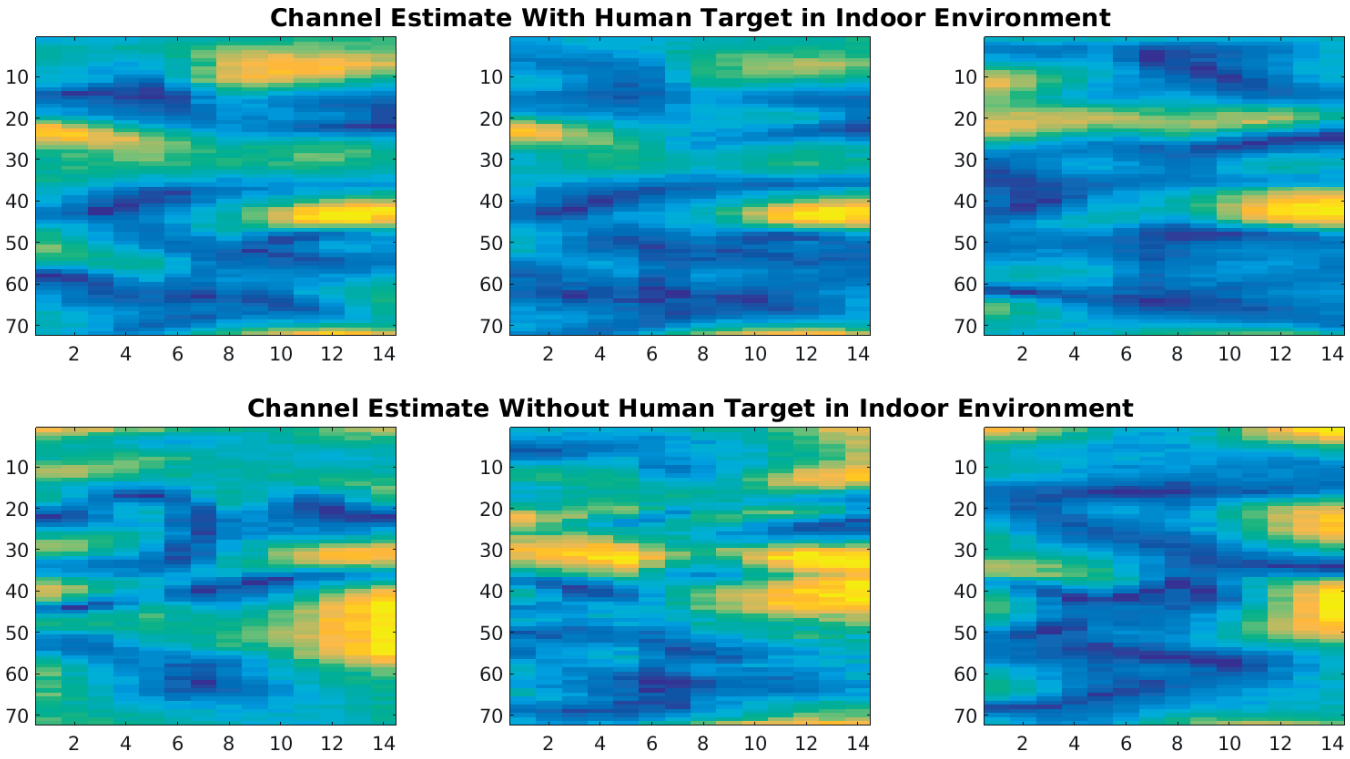

Figure 10.
Multiple channel estimates with and without a human target in an indoor environment. The top row represents channel estimates with the human target in the indoor environment, and the bottom row corresponds to channel estimates without the human target in the indoor environment.

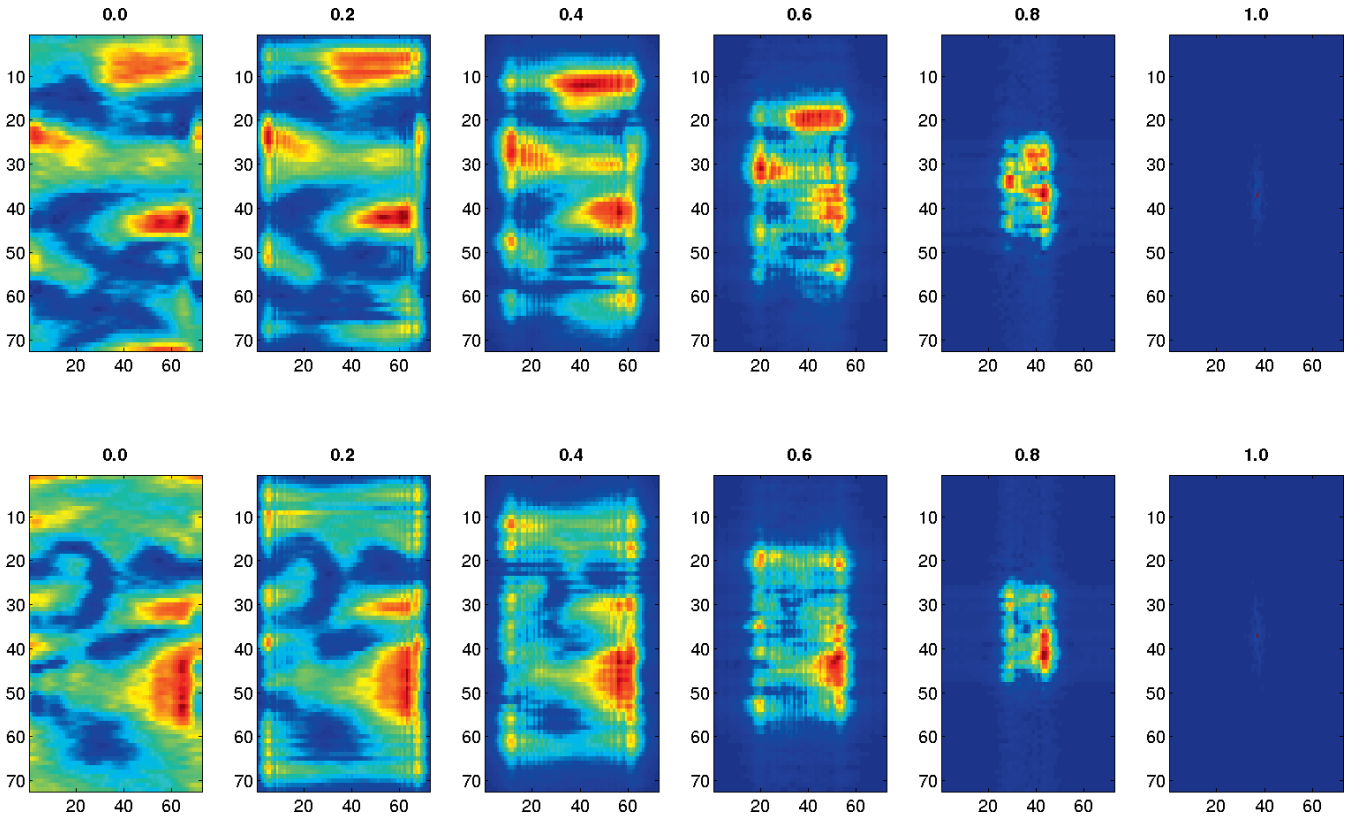

Figure 11.
FrFT representations of channel estimates for with (row 1) and without (row 2) human-target cases for different rotation angles (a radian).

Figure 12.
Human target present in the indoor environment at different distances from the SDR platform.

in the case of rotation angle $a = 0.6$. Therefore, TFR for $a = 0.6$ can be used to visually distinguish the presence of a human in an indoor environment from the absence of a human.

Effect of Varying the Distance of the Object from the Sensing System

The objective of this experiment is to find the effect of changing the distance of the object, i.e., the human target in this experiment, on the distinguishing capability of LTE CommSense in an indoor environment. The following experimental procedure was adopted for this purpose:

1. Four distances of the human target from the SDR platform in indoor environments were chosen.
2. LTE DL signals were captured with and without the human target for those four distances, keeping the indoor background fixed. Figure 12 shows the two distances of the human target from the SDR in the indoor environment.
3. Five readings were taken, viz. one for only the background with no human target present and the other four corresponding to a human target present at four distances: 0.5, 1, 2, and 3 m.
4. The channel estimates for all cases were evaluated.
5. PCA was performed on the dataset for dimensionality reduction.

To select how many principal components are sufficient for this case, the sorted eigenvalues and their cumulative energy contribution are plotted in Figure 13a. The largest two principal components are plotted in a 2D scatterplot and shown in Figure 13b. The largest three principal components are plotted in a 3D scatterplot and shown in Figure 13c. In the scatterplots in Figure 13, "black dots" and "blue circles" represent the lowest distances (i.e., 0.5 and 1 m). "Cyan crosses" represent a distance of 2 m, the "green *X*" is for a distance of 3 m, and "magenta squares" are representative of no human target present in the scene. Five clusters can be observed for the five cases. It can be further observed that the distance between the cluster centers decreases as the distance of the human target from the SDR platform increases.

Next, SVM-based classification was performed on the collected data, corresponding to the two datasets, i.e., with human target and without human target. For the different datasets, the distance of the human target from the SDR platform varies. Separate training and testing datasets were prepared to find the detection accuracy and corresponding confusion matrix. The nomenclature of different test cases generated from the database is as follows: *Case$b-r$r*. Here, *$b* is the sequence number of the indoor background being considered and *r* denotes the number of readings for the considered background. For example, *Case*3-*r*100 is the third dataset of 100 readings with and without a human target. Here, the human target is at a particular distance from the CommSense receiver platform.

For each of the preceding cases, the performance accuracy and confusion matrix were evaluated. An average recognition accuracy of 88.9% was achieved in this case.

The two standard measures to indicate the identifying power of a detection methodology are false rejection rate (FRR) and false acceptance rate (FAR) [20], [21]. FRR is considered a type I error, and FAR is considered a type II error. FAR is fraction of the falsely accepted patterns (i.e., human target not present but classified as human target present) divided by the number of all impostor patterns. The fraction of the number of rejected client patterns (i.e., human target present but not detected) divided by the total number of client patterns is the FRR. According to Bolle et al. [20], false accept (FA) is an act of deciding that a category is legitimate when it is an impostor in reality. The frequency at which FA errors are made can be denoted as FAR. If NFA signifies the number

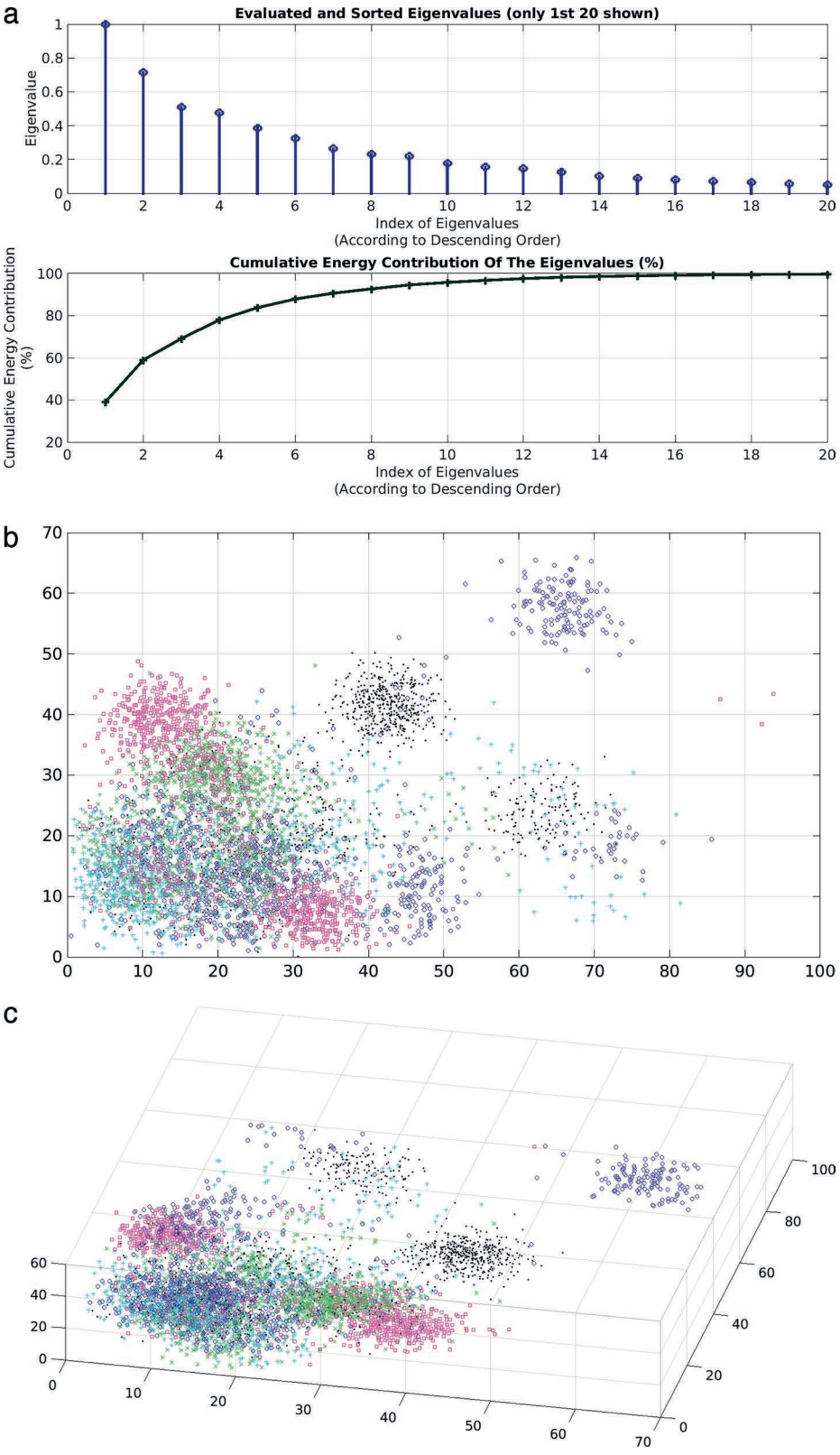

Figure 13.
Indoor human-target detection at different distances: (a) sorted eigenvalues and their cumulative energy contribution, (b) 2D scatterplot of the largest two principal components, (c) 3D scatterplot of the largest three principal components.

of false acceptances and NIA denotes the number of impostor attempts, then FAR can be defined as follows:

$$\mathrm{FAR} = \left(\frac{\mathrm{NFA}}{\mathrm{NIA}}\right) * 100\%$$

Similarly, false reject (FR) is the act of deciding that a category is not legitimate when the category is genuine in reality. The frequency at which FR errors are made is called FRR. If NFR is the number of failed rejections and NEA is the number of legitimate classification attempts, then FRR can be given as follows:

$$\mathrm{FRR} = \left(\frac{\mathrm{NFR}}{\mathrm{NEA}}\right) * 100\%$$

A good detection methodology should optimize both FAR and FRR. Figure 14 shows the FRR and FAR values with respect to the distance of the human target from the SDR platform. It can be observed that as the distance of the human target from the SDR platform decreases, the FAR and FRR values improve.

The following interesting points can be observed:

- Even with a training set consisting of only 100 readings, the performance is good when tested with up to 1,000 readings.
- As the distance of the human target from the SDR decreases, the accuracy and the FAR and FRR performance improve.

From the confusion matrix, the average FRR and FAR are calculated as follows:

- Type I error: FRR = 4.56%
- Type II error: FAR = 3.57%

Analyzing the effect of the distance of the human target from the LTE UE to detect human presence, it can be concluded that for four human-target distances and the case with only background, they form separate clusters and that the distance of cluster centers from the cluster correspond-

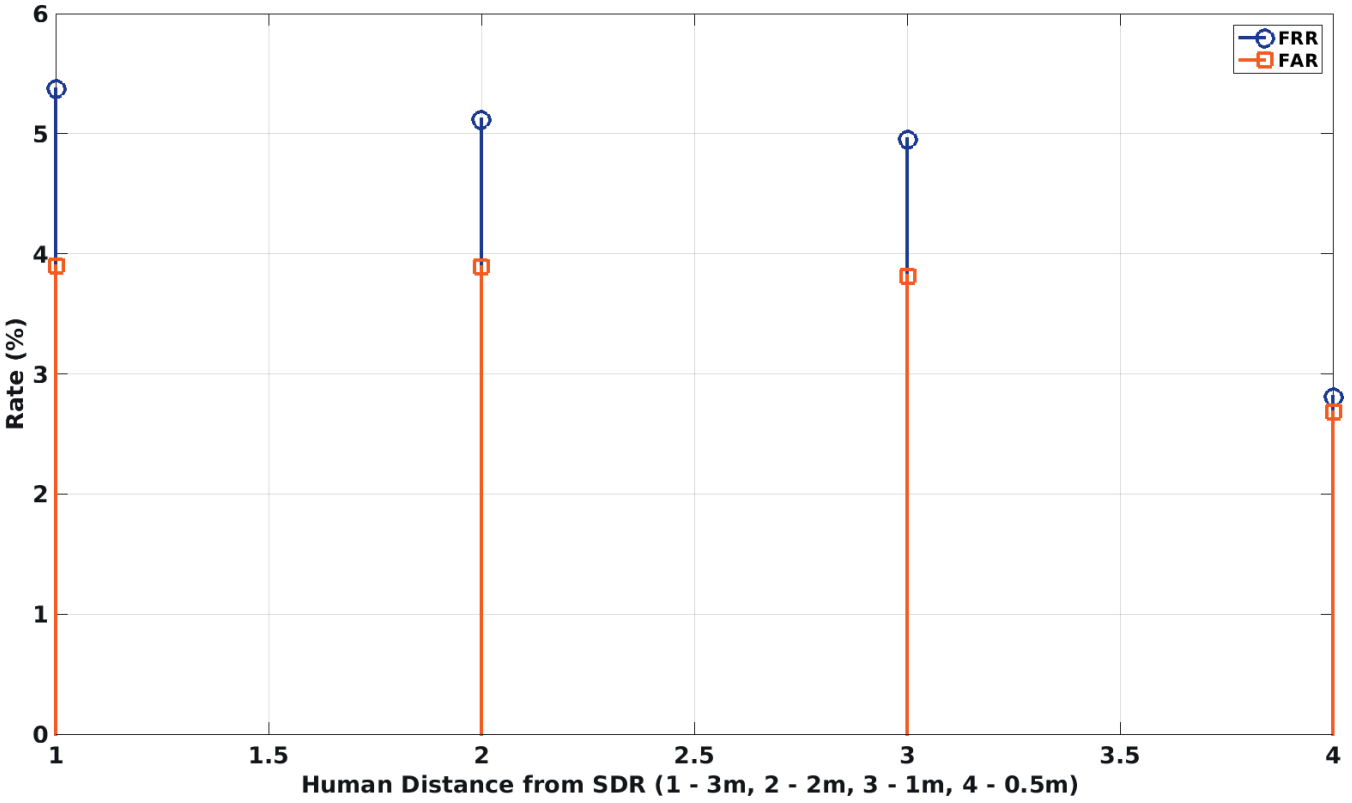

Figure 14.
FRR and FAR percentage at different distances (3, 2, 1, and 0.5 m) of the human target from the LTE CommSense SDR platform.

ing to indoor background decreases as the distance of the human target from the UE increases.

CONCLUSION

This research is intended to contribute to the field of telecommunication-based environment sensing. The proposed system being essentially a commensal radar, it does not affect the existing telecommunication system. Hence, the required effort is less, and it will be a cost-effective solution. Contrary to conventional radar, which accurately measures the range of a target in the scene, LTE CommSense can be used to detect and characterize environment changes.

To establish the preceding claim, first the LTE CommSense hypothesis was proved in a simulation environment. It was shown that different ITU-specified channel models can be clearly distinguished using the LTE CommSense system model. Next, practical LTE DL data were captured in an indoor environment with and without a human target with the intention of detecting the human using CommSense. Multiple channel estimates were evaluated with and without a human in indoor situations. Their dimensionality was reduced using PCA and plotted in 2D and 3D scatterplots. Those plots revealed that with-human cases and without-human cases form different clusters. In another attempt to visually distinguish the two cases, FrFT was performed on the channel estimates for different rotation angles and corresponding TFRs were plotted. Though the difference between the two cases was visible for all angles, it was prominent in the case of rotation angle $a = 0.6$. The final attempt was to investigate the effect of changing the distance of the human target on the distinguishing capability of LTE CommSense in an indoor environment. It was observed that for four distances and the case with only an indoor background, they formed separate clusters and that the distance of the cluster centers from the cluster corresponding to the indoor background decreased as the distance of the human from the UE increased.

The simulation and experiments with field-collected data support the claim that LTE CommSense is useful in detecting and characterizing environment changes. A human target in an indoor environment is detected in this work in support of the claim. In the future, the capability of LTE CommSense to detect environment changes in an outdoor environment may be investigated. The possibility of through-the-wall detection with this instrumentation may also be explored. ◈

REFERENCES

[1] Rittenbach, O. E. Communication by radar beams, U.S. Patent 3 460 139, Aug. 5, 1969.

[2] Griffiths, H., and Baker, C. Passive coherent location radar systems. Part 1: performance prediction. *IEE Proceedings: Radar, Sonar and Navigation,* Vol. 152, 3 (2005), 153–159.

[3] Inggs, M., and Tong, C. Commensal radar using separated reference and surveillance channel configuration. *Electronics Letters,* Vol. 48, 18 (2012), 1158–1160.

[4] Bhatta, A., and Mishra, A. K. Implementation of GSM channel estimation using open-source SDR environment. In *2015 International Conference on Microwave, Optical and Communication Engineering (ICMOCE),* Dec. 2015, 322–325.

[5] Bhatta, A., and Mishra, A. GSM based CommSense system to measure and estimate environmental changes. *IEEE Aerospace and Electronic Systems Magazine,* to be published.

[6] Howland, P., Maksimiuk, D., and Reitsma, G. FM radio based bistatic radar. *IEE Proceedings: Radar, Sonar and Navigation,* Vol. 152, 3 (June 2005), 107–115.

[7] Mishra, A. K. CommSense: Radar system using existing communication infrastructure to sense the environment. In *Proceedings of the 25th IEEE International Radioelektronika Conference,* 2015, 276–279.

[8] Amit, M. K. Monitoring changes in an environment by means of communication devices, UK IP Office, Patent Application GB1506665.7, Apr. 20, 2015.

[9] Huang, T., and Zhao, T. Low PMEPR OFDM radar waveform design using the iterative least squares algorithm. *IEEE Signal Processing Letters,* Vol. 22 (2015), 1975–1979.

[10] Huynen, J. R. A revisitation of the phenomenological approach with applications to radar target decomposition. DTIC Document, Tech Rep., 1982.

[11] Mishra, A. K. Application specific instrumentation (ASIN): a bio-inspired paradigm to instrumentation using recognition before detection, submitted for publication, abs/1611.00228.

[12] Sesia, S., Toufik, I., and Baker, M. *LTE—The UMTS Long Term Evolution, From Theory to Practice*. West Sussex, UK:Wiley, 2009.

[13] Yun, S., and Qiu, L. Supporting WiFi and LTE co-existence. In *Proceedings of the IEEE Conference on Computer Communications (INFOCOM),* Apr. 2015, 810–818.

[14] Nikaein, N., Knopp, R., Kaltenberger, F., Gauthier, L., Bonnet, C., Nussbaum, D., and Ghaddab, R. Demo: OpenAirInterface: An open LTE network in a PC. In *Proceedings of the 20th Annual International Conference on Mobile Computing and Networking,* Maui, Hawaii, Sep. 7–11, 2014. [Online]. Available: http://www.eurecom.fr/publication/4371.

[15] Ettus Research. USRP N200/N210 networked series, http://www.ettus.com/product/category/Daughterboards/RFX2400.

[16] Ettus Research. USRP N200/N210 networked series. http://www.ettus.com/product/details/VERT2450.

[17] Mishra, A., and Sardar, S. An improved algorithm for UWB based imaging of breast tumors. In *Proceedings of the International Conference on Image Information Processing (ICIIP-2011),* Nov. 2011.

[18] Ozaktas, H. M., Zalevsky, Z., and Kutay, M. A. *The Fractional Fourier Transform: With Applications in Optics and Signal Processing*. West Sussex, UK: John Wiley & Sons, 2001.

[19] Sardar, S., and Mishra, A. K. A robust and efficient SAR ATR algorithm using a hybrid model of fractional Fourier transform and pulse coupled neural network. In *Proceedings of the IEEE International Microwave and RF Conference (IMaRC),* Dec. 2014, 121–124.

[20] Bolle, R., Connell, J., Pankanti, S., Ratha, N., and Senior, A. *Guide to Biometrics (Springer Professional Computing)* (1st ed.). New York, NY:Springer, Nov. 2003.

[21] Sardar, S., Tewari, G., and Babu, K. A. A hardware/software co-design model for face recognition using cognimem neural network chip. In *Proceedings of the International Conference on Image Information Processing,* Nov. 2011, 1–6.